2-P

NASA TECHNICAL MEMORANDUM

NASA TM X- 68229

NASA TM X- 68229

A SIMPLIFIED FUEL CONTROL APPROACH FOR LOW COST AIRCRAFT GAS TURBINES

by Harold Gold
Lewis Research Center
Cleveland, Ohio

TECHNICAL PAPER proposed for presentation at
National Air Transportation Meeting sponsored by
the Society of Automotive Engineers
Miami, Florida, April 24-26, 1973

A SIMPLIFIED FUEL CONTROL APPROACH FOR LOW COST AIRCRAFT GAS TURBINES

by Harold Gold

Lewis Research Center
National Aeronautics and Space Administration
Cleveland, Ohio

ABSTRACT

Cost reduction in aircraft turbine engines may be obtained through performance reductions that are acceptable for ranges that are considerably shorter than the range for which current and costly engines were developed. Cost reduction in the fuel control for these cost engines must be achieved without significant performance reduction. This paper describes a fuel control approach that appears to meet this requirement and reviews the work that has been performed on it over the past few years.

INTRODUCTION

Recent developments in missle technology, such as in the Navy Harpoon program, clearly demonstrate that important mission requirements can be met with simple, fixed geometry turbine engines. For short range missions of this type a basic engine design procedure is to reduce pressure ratio until the range margin is reached. The simplest engine thus arrived at is nevertheless a very high rotative speed machine and is required, from size and weight limitations, to operate very near thermal and structural limits. Because of this level of operation and the logistic requirement for reliability, the control requirements remain substantially as high as on complex engines. Even in the possible application of low cost engine technology to man-rated, general aviation aircraft, where thermal

and structural margins would be greater, the reliability requirement would also be greater. Therefore, there does not appear to be an application in which reduction in complexity and cost in fuel controls can be traded for ineffective or inaccurate control.

Reduction in the complexity of gas turbine fuel controls without loss of control accuracy, reliability or effectiveness has been a goal in the low cost technology program at Lewis Research Center. This paper presents a description and analysis of a hydromechanical approach that has been studied in the Lewis Program and which appears from analysis and test to have met this requirement. A computer simulation of the control mechanism is given in Ref. 1 and performance of a physical model in engine test is reported in Ref. 2. A second physical model is currently in use in experimental operation of a low-cost ordnance-technology engine, under a joint Lewis-Naval Weapons Center program. A computer study of this engine and control is reported in Ref. 3.

SYMBOLS

A_B	bypass orifice area
A_G	governor valve orifice area
A_R	speed sensing orifice area
A_S	low speed valve orifice area
A_2	P_2 absolute valve orifice area
A_{3a}	$(P_3 - P_2)$ valve acceleration orifice area
A_{3d}	$(P_3 - P_2)$ valve deceleration orifice area
C_t	turbine constant
c_p	specific heat
D	speed sensing pump displacement, vol./%N
e	flow error, percent

H	heating value
K_a	acceleration constant
K_e	engine constant
K_s	steady state constant
N	engine speed, percent of design
P'_a	speed sensing pump inlet pressure
P_a	speed sensing pump discharge pressure
P_{STD}	standard pressure
ΔP_R	regulated pressure error
P_2	engine inlet total pressure
P_3	compressor discharge total pressure
Q	volumetric flow rate
R	constant
R_L	pump leakage resistance
r_c	compressor pressure ratio
r_t	turbine pressure ratio
T_2	engine inlet temperature absolute
T_4	turbine inlet temperature absolute
w_a	engine airflow
w_c	compressor airflow
w_f	fuel mass flow rate
w_t	turbine gas flow
γ_c	ratio of specific heats, compressor
γ_t	ratio of specific heats, turbine
δ	ratio of pressure to NACA standard sea-level pressure

θ ratio of temperature to NACA standard sea-level temperature

ρ fuel density

GENERALIZED ACCELERATION AND DECELERATION CONTROL PARAMETERS

As developed in Appendix A, the relationship between the engine variables corrected speed, corrected fuel flow, and pressure ratio under zero ram is approximately

$$\frac{w_f/\delta\sqrt{\theta}}{N/\sqrt{\theta}} = (K_s)\frac{P_3}{P_2} \tag{1}$$

and the relationship between corrected fuel flow-acceleration increment, corrected speed and pressure ratio, for constant torque acceleration is approximately

$$\frac{\Delta w_f/\delta\sqrt{\theta}}{N/\sqrt{\theta}} = K_a = \frac{K_e c_p P_{STD}}{H} \cdot \frac{\Delta T_4}{T_2} \tag{2}$$

Summing Eqs. (1) and (2) gives the relationship between these variables for the constant torque acceleration fuel flow.

$$\frac{w_f\,acc/\delta\sqrt{\theta}}{N/\sqrt{\theta}} = K_a + (K_s)\frac{P_3}{P_2} \tag{3}$$

Equation (3) gives the relationship for constant torque deceleration fuel flow when ΔT_4 is made negative. An alternate deceleration limit is a fixed fraction of the steady state flow. This limit is expressed

$$\frac{w_f/\delta\sqrt{\theta}}{N/\sqrt{\theta}} = \left(\frac{K_s}{R}\right)\frac{P_3}{P_2}, \qquad R > 1 \tag{4}$$

In the corrected parameter plane, Fig. 1, the steady state engine characteristic forms a straight line through the origin and similarly the deceleration limit. The constant torque acceleration limit forms a line that is above and parallel to the steady state line. The magnitude of the intercept K_a is limited by compressor surge and/or maximum allowable T_4 and the intercept $(-K_a)$ or the factor R are limited by combustor blow-out.

CONTROL METHOD

Basic hydromechanical metering circuit. - A schematic drawing of the circuit that is employed to function in accordance with the generalized parameters is shown in Fig. 2. In this circuit, the free piston pressure regulator returns excess flow from the fuel pump to hold the pressure gradient across the speed sensing pump at zero. The regulator senses the speed sensing pump downstream pressure at the junction between the pump and the speed sensing orifice. By minimizing the volume in this junction the hydraulic impedance of the junction is kept high, through which a stable regulator is readily obtained. By virtue of the regulated equality of the pressures P_a' and P_a, the pressure drop across the bypass orifice is made equal to the pressure drop across the speed sensing orifice. The flow output, being the sum of the two orifice flows is:

$$w_f = \rho DN\left[\frac{A_B}{A_R} + 1\right] \tag{5}$$

Flow from the P_a' junction to the return annulus, through the piston clearance, is blocked by the leak blocking annulus, the pressure

in which is P_a. This leak blocking technique is also used on the speed sensing pump drive shaft. The flow into the speed sensing orifice can therefore be accurately proportional to engine speed and the output flow according to Eq. (5) is independent of the discharge pressure P_b. It will be noted that the output is a product of speed and a function of three other variables ρD, A_R and A_B. When ρD and A_R are fixed, the pressure drop across A_R is proportional to the square of speed. This speed signal can be utilized to vary A_B to obtain a governing action. Because flow from the speed sensing pump is an independent speed signal, A_R can also be varied as a function of speed. In addition A_B can be varied from other inputs and be in the form of series-parallel networks to obtain an output that is a complex function of many variables. A brief error analysis of this circuit is given in Appendix B.

VARIABLE ORIFICE NETWORK

Speed governing. - The overall system schematic drawing of the fuel control, Fig. 3 illustrates the series-parallel orifice network. The flow passages are so connected that the governer orifice A_G is in series with the parallel orifices A_{3a}, A_2 and A_s, and is in parallel with the orifice A_{3d}. The maximum value of A_G is large compared to the sum of $A_{3a} + A_2 + A_s$. For this reason, the flow through these orifices is unaffected by A_G when the governor valve is driven to its open limit. In an acceleration transient A_G is driven toward closed by the pressure difference $(P_a - P_b)$ when the set speed is approached. At the set speed the area of the bypass orifice network is such that the flow, according to Eq. (5), equals the engine steady state fuel flow.

The use of the speed feedback signal $(P_a - P_b)$ instead of its equal $(P'_a - P_b)$ eliminates interaction between the governor valve and the speed signal. However, the P_a signal provides very little governor damping and a governor damping orifice is required. The governor damping orifice diameter is set to give the valve spring-mass system an effective 0.5 damping ratio. The governor valve port is contoured so that A_G varies

logarithmically with stroke, through which the governor-engine loop gain is held within stability limits over the engine speed range. The reduction in the value of A_{3a} and A_2 with altitude reduces the governor orifice gain and provides altitude adjustment of the loop gain and attenuation of steady state speed droop with altitude.

Starting control. - As illustrated in Fig. 3, the low speed valve is actuated by the speed signal $(P_a - P_b)$ and its orifice is in series with the governor orifice. This valve provides an increase in the acceleration limit in the starting speed range. The value of A_s is driven to zero at approximately idle speed. Under low speed starting conditions the area A_s is large compared to the sum A_{3a}, A_{3d} and A_2. For this reason the starting flow is essentially independent of altitude. On an engine that utilizes fixed area fuel nozzles, the fixed starting flow provides constant atomization quality at altitude. This starting component is currently employed in the fuel control model that is on the Low Cost Ordnance Technology engine.

On an engine that is equipped with a dual fuel nozzle system, constant fuel-air ratio is required for ignition. The modulation of starting flow to hold the starting fuel air ratio constant with altitude can be obtained through the use of a variable speed sensing orifice. In the configuration depicted in Fig. 3, a fixed speed sensing orifice is in the head of a piston. The orifice is partially closed by a cone under cranking speeds and is moved away from the cone as speed increases by the pressure drop $(P'_a - P_b)$. The speed sensing orifice remains fixed above idle speed. This starting component was employed on the control model reported in Ref. 2.

Variable orifice relations for acceleration and deceleration limits. - From Eq. (3), the acceleration limit is

$$w_f = N\left[\left(\frac{K_s}{P_{STD}}\right)P_3 + \left(\frac{K_a}{P_{STD}}\right)P_2\right] \tag{6}$$

or in terms of one absolute pressure

$$w_f = N\left[\left(\frac{K_s}{P_{STD}}\right)(P_3 - P_2) + \left(\frac{K_s + K_a}{P_{STD}}\right) P_2\right] \tag{7}$$

The area of the bypass orifice network, at fixed speed sensing orifice area, to give the acceleration limit that is defined by Eq. (7) is found by equating the right sides of Eqs. (5) and (7).

$$A_{Ba} = \left[\frac{A_R K_s}{\rho D P_{STD}}\right](P_3 - P_2) + \left[\frac{A_R(K_s + K_a)}{\rho D P_{STD}}\right] P_2 - A_R \tag{8}$$

From Eq. (4), the deceleration limit is

$$w_f = N\left[\frac{K_s}{R P_{STD}}\right] P_3 \tag{9}$$

or in terms of the pressure difference $(P_3 - P_2)$

$$w_f = N\left[\left(\frac{K_s}{R P_{STD}}\right)(P_3 - P_2) + \left(\frac{K_s}{R P_{STD}}\right) P_2\right] \tag{10}$$

The area of the bypass orifice network, at fixed speed sensing orifice area, to give the deceleration limit that is defined by Eq. (10) is found by equating the right side of Eqs. (5) and (10).

$$A_{Bd} = \left[\frac{A_R K_s}{R\rho D P_{STD}}\right](P_3 - P_2) + \left[\frac{A_R K_s}{R\rho D P_{STD}}\right] P_2 - A_R \tag{11}$$

The term $\left[A_R K_s / R\rho D P_{STD}\right] P_2 - A_R$ in Eq. (11) is relatively small and can be either neglected or treated as a constant. In this analysis it will

be treated as a constant. Setting $P_2 = P_{2c}$ (constant) in Eq. (11) and substituting Eq. (11) for A_B in Eq. (5), the deceleration limit is found to be

$$\frac{w_f/\delta\sqrt{\theta}}{N/\sqrt{\theta}} = \left[\frac{K_s}{R}\right]\left(\frac{P_3}{P_2}\right) + K_s\left(\frac{P_{2c}}{P_2} - \frac{1}{R}\right) \tag{12}$$

As indicated by Eq. (12), the deceleration limit so defined is enriched as P_2 is reduced. From Ref. 1, the order of this effect is as shown in Fig. 4. According to Eq. (12), the bypass area is

$$A_{Bd} = \left[\frac{A_R K_s}{R\rho D P_{STD}}\right](P_3 - P_2) + A_R\left[\frac{K_s P_{2c}}{R\rho D P_{STD}} - 1\right] \tag{13}$$

Speed sensing pump displacement. - The speed sensing pump displacement is selected to permit the system to function in accordance with Eq. (8) at the lowest expected value of P_2. This is found by setting the Eq. (8) term

$$\left[\frac{A_R(K_s + K_a)}{\rho D P_{STD}}\right] P_{2min} - A_R = 0$$

From which

$$\rho D = \left(\frac{K_s + K_a}{P_{STD}}\right) P_{2min} \tag{14}$$

Substituting Eq. (14) in Eq. (8)

$$A_{Ba} = \left[\frac{A_R K_s}{(K_s + K_a)P_{2min}}\right](P_3 - P_2) + \left[\frac{A_R}{P_{2min}}\right] P_2 - A_R \tag{15}$$

Substituting Eq. (14) in Eq. (13)

$$A_{Bd} = \left[\frac{A_R K_s}{R(K_s + K_a)P_{2min}}\right](P_3 - P_2) + A_R\left[\frac{K_s P_{2c}}{R(K_s + K_a)P_{2min}} - 1\right] \quad (16)$$

$(P_3 - P_2)$ and P_2 valves. - At speeds above idle, the acceleration limit is controlled by the sum $(A_{3a} + A_{3d} + A_2)$, and the deceleration limit is controlled by the value of A_{3d}. It is therefore required that

$$A_{3d} = A_{Bd}$$

or

$$A_{3d} = \left[\frac{A_R K_s}{R(K_s + K_a)P_{2min}}\right](P_3 - P_2) + A_R\left[\frac{K_s P_{2c}}{R(K_s + K_a)P_{2min}} - 1\right] \quad (17)$$

The second requirement is

$$A_{3a} + A_2 = A_{Ba} - A_{Bd}$$

or

$$A_{3a} + A_2 = \left[\left(\frac{A_R K_s}{(K_s + K_a)P_{2min}}\right)\left(1 - \frac{1}{R}\right)\right](P_3 - P_2) +$$

$$+ \left[\frac{A_R}{P_{2min}}\right]P_2 - \frac{A_R K_s P_{2c}}{R(K_s + K_a)P_{2min}} \quad (18)$$

From Eq. (18)

$$A_{3a} = \left[\left(\frac{A_R K_s}{(K_s + K_a)P_{2min}}\right)\left(1 - \frac{1}{R}\right)\right](P_3 - P_2) \tag{19}$$

and

$$A_2 = \left[\frac{A_R}{P_{2min}}\right]P_2 - \frac{A_R K_s P_{2c}}{R(K_s + K_a)P_{2min}} \tag{20}$$

The value of P_{2c} is found from Eq. (20) by setting $P_2 = P_{2min}$ and $A_2 = 0$

$$P_{2c} = \frac{R(K_s + K_a)P_{2min}}{K_s} \tag{21}$$

Substituting Eq. (21) in Eq. (20)

$$A_2 = \left[\frac{A_R}{P_{2min}}\right]P_2 - A_R \tag{22}$$

Substituting Eq. (21) in Eq. (17)

$$A_{3d} = \left[\frac{A_R K_s}{R(K_s + K_a)P_{2min}}\right](P_3 - P_2) \tag{23}$$

Substituting Eq. (21) in Eq. (12)

$$\frac{w_f/\delta\sqrt{\theta}}{N/\sqrt{\theta}} = \left[\frac{K_s}{R}\right]\left(\frac{P_3}{P_2}\right) + \left[\frac{R(K_s + K_a)P_{2min}}{P_2} - \frac{K_s}{R}\right] \tag{24}$$

Equations (14), (19), (21), (22), and (23) are the basic design equations of the system. It will be noted that for $R = 2$ $A_{3a} = A_{3d}$.

Valve construction. - The valve spools and sleeves have been fabricated from hardened stainless steel in the physical models that have been built thus far. Valve displacement gains have been 0.002 in./psi to 0.005 in./psi. With these gains the spring-mass natural frequencies have been above 100 cps. Slots formed in the sleeves coact with the spool lands to form the variable orifice. The slots, which have been formed by EDM have been from 0.03 in. to 0.10 in. wide. The maximum orifice pressure drop has been 50 psi. Because of the low pressure drop, flow forces and spool-sleeve leakage has been very small. With the construction indicated in Fig. 2, spool leakage flows into the P_2 and P_3 lines. This leakage flows into the engine and has not appeared to be a problem. The leakage can be eliminated through the use of bellows at each end of the $(P_3 - P_2)$ and P_2 valves.

Bench adjustment of the valve bias screws is made at a fixed speed that is sufficiently above idle to assure closure of the low speed valve and/or fixed position of the variable speed sensing orifice. The $(P_3 - P_2)$ valve adjustment is made first with the governor valve in closed position. In this condition A_{3d} is varied to satisfy Eq. (24). The governor valve is then moved to its maximum opening and the P_2 valve is adjusted to satisfy Eq. (3).

CONTROL PERFORMANCE

Performance on the J-85 engine. - In the study reported in Ref. 1 the control mechanism of pump and variable orifice network was simulated on an analog computer and was used to control both a computer simulated and an actual engine. In the control of the actual engine, the computer responded to speed and pressure sensors installed on the engine and varied fuel flow through a high response, electrohydraulic flow regulator. The engine tests were conducted only under sea level static conditions. The examination of altitude ram operation was performed in the simulated engine mode.

Operation in the corrected parameter plane at sea level and at altitude is shown in Fig. 5. The relation between the engine steady state operating line and the acceleration and deceleration limits at altitude is shown to be comparable with that at sea level. The lines between the limits are the fixed throttle governor operating lines.

Acceleration of the actual engine at sea level is shown in Fig. 6, and acceleration of the simulated engine at 40 000 ft, Mach 0.90 is shown in Fig. 7. The constant torque characteristic and the high gain but stable governor action is evident in the speed and fuel flow traces.

The barometric compensation of the proportional governor by the $(P_2 - P_3)$ and the P_2 valves is illustrated in Fig. 8. As indicated, the engine speed increases from 97.5 percent to 100 percent in going from sea level static to 40 000 ft, Mach 0.9.

Installation of the physical model of this control on the J-85 engine is shown in Fig. 9. This was a bread-board model and no attempt was made to conserve bulk. A photograph of the valve spools and the pump and regulator components is shown in Fig. 10. The variable orifice slots are carried in the valve spools rather than in the sleeves in the configuration. The action of the variable speed orifice that is used to provide starting control in this model is shown in Fig. 11. Engine start is shown in Fig. 12, where rapid acceleration and lack of exhaust gas temperature over-shoot is evident in the oscillograph traces. Engine acceleration is shown in Fig. 13 and deceleration is shown in Fig. 14. The similarity of the performance of the simulated and the physical model is evident in both the acceleration time and the governor action.

Performance on the Low Cost Ordnance Technology engine. - Figure 15, taken from the computer study reported in Ref. 3, shows the effect of flight speed in the corrected parameter plane. As shown, flight speed rotates the steady-state engine operating line towards the deceleration limit at low engine speeds. In this instance, the Mach 0.9 operating line intersects the deceleration limit at approximately 70 percent speed, but this is beyond a realistic operation condition.

B

Installation of the fuel control on the Low Cost Ordnance Technology engine is shown in Fig. 16. This control model is packaged for small bulk and contains the fuel pump. The fuel pump and the speed sensing pump are driven through a common shaft which is driven to a maximum speed of 7400 rpm by a gear box which is in the front housing hub. Figure 17 is a photograph of the valve spools and sleeves, speed sensing pump gears and the pressure regulator piston.

Figure 18 is a bench calibration of the fuel control plotted on the coordinates of flow rate against engine speed. The rise in the acceleration limit caused by the action of the low speed valve is evident. The increasing slope of the governor operating lines with speed is employed to hold the loop gain nearly constant over the speed range.

Start of this engine is shown in Fig. 19 and acceleration in Fig. 20. The similarity of the high gain governor action in these accelerations with the J-85 test results is evident.

CONCLUDING REMARKS

The aim of this program has been to demonstrate principle and technical feasibility rather than to qualify a particular design. Accordingly there is no data available on environmental or life tests. This paper has been presented to contribute to the advancement of gas turbine fuel control technology and to promote both simplification and reduction in cost.

APPENDIX A

A DERIVATION OF THE GENERALIZED CONTROL PARAMETERS

Engine steady-state approximation. - In steady state, the equality of compressor and turbine power at equal component efficiencies can be expressed

$$\left(\frac{w_t \gamma_t}{\gamma_t - 1}\right) T_4 \left\{1 - \left(\frac{1}{\gamma_t}\right)^{\gamma_t - 1/\gamma_t}\right\} = \left(\frac{w_c \gamma_c}{\gamma_c - 1}\right) T_2 \left\{\gamma_c^{\gamma_c - 1/\gamma_c} - 1\right\} \tag{A1}$$

Introducing the average values of $\gamma_t = 1.32$ and $\gamma_c = 1.4$, the turbine inlet temperature is given by

$$T_4 = 0.83\, T_2\, r_t^{0.244}\, \frac{\left(r_c^{0.286} - 1\right) w_c}{\left(r_t^{0.244} - 1\right) w_t} \tag{A2}$$

For values of pressure ratios between two and six the linear approximations of the $(r^{\gamma - 1/\gamma} - 1)$ terms are

$$(r^{0.286} - 1) = 0.117r$$

$$(r^{0.244} - 1) = 0.097r$$

With these approximations Eq. (A2) becomes

$$T_4 = \left(\frac{r_c w_c}{r_t w_t}\right) T_2 r_t^{0.244} \tag{A3}$$

Introducing the further approximations appropriate to this pressure ratio range

$$w_c = w_t$$

and

$$r_c = r_t^{1.5}$$

Equation (A3) becomes

$$T_4 = T_2 r_c^{0.495} \tag{A4}$$

In terms of the energy input

$$T_4 = T_2 r_c^{0.286} + \frac{H}{c_p}\frac{w_f}{w_a} \tag{A5}$$

Eliminating T_4 between Eqs. (A4) and (A5)

$$w_f = \frac{w_a c_p T_2}{H}\left(r_c^{0.495} - r_c^{0.286}\right) \tag{A6}$$

The linear approximation of the exponential term is

$$\left(r_c^{0.495} - r_c^{0.286}\right) = 0.122\, r_c$$

With this approximation Eq. (A6) becomes

$$w_f = \left(\frac{0.122 w_a c_p T_2}{H}\right)\frac{P_3}{P_2} \tag{A7}$$

Engine air flow is closely proportional to the product of speed and inlet density.

$$w_a = \frac{K_e N P_2}{T_2} \tag{A8}$$

Substituting Eq. (A8) in (A7)

$$w_f = \frac{0.122 K_e c_p N P_3}{H} \tag{A9}$$

or

$$\frac{w_f}{N P_2} = \left[\frac{0.122 K_e c_p}{H}\right] \frac{P_3}{P_2} \tag{A10}$$

From which the general relation is

$$\frac{w_f/\delta\sqrt{\theta}}{N/\sqrt{\theta}} = (K_s) \frac{P_3}{P_2} \tag{A11}$$

Constant torque acceleration. - The turbine torque may be expressed

$$Q_T = C_T \frac{w_a}{N} T_4 \left[1 - \left(\frac{1}{\gamma_t}\right)^{\gamma_t - 1/\gamma_t}\right] \tag{A12}$$

Substituting Eq. (A8)

$$\frac{Q_T}{P_2} = C_T K_e \left[1 - \left(\frac{1}{\gamma_t}\right)^{\gamma_t - 1/\gamma_t}\right] \frac{T_4}{T_2} \tag{A13}$$

The acceleration torque which is obtained by increasing T_4 is, from Eq. (A13)

$$\frac{\Delta Q_T}{P_2} = C_T K_e \left[1 - \left(\frac{1}{\gamma_t}\right)^{\gamma_t - 1/\gamma_t}\right] \left(\frac{T_{4\,acc} - T_{4\,ss}}{T_2}\right)$$

From which the general relation is

$$\frac{\Delta Q_T}{\delta} = \frac{P_{STD} C_T K_e}{T_{STD}} \left[1 - \left(\frac{1}{\gamma_t}\right)^{\gamma_t - 1/\gamma_t}\right]\left(\frac{\Delta T_4}{\theta}\right) \tag{A14}$$

Over the major portion of the engine speed range the adiabatic term in Eq. (A14) is substantially constant and therefore the corrected torque is approximately proportional to the corrected increment in T_4.

The required increment in fuel flow for an increment ΔT_4 is

$$\Delta w_f = \frac{C_p w_a \Delta T_4}{H} \tag{A15}$$

Substituting Eq. (A8)

$$\Delta w_f = \frac{C_p K_e N P_2 \Delta T_4}{H T_2}$$

or

$$\frac{\Delta w_f}{P_2\sqrt{T_2}} = \frac{C_p K_e}{H} \frac{\Delta T_4}{T_2} \frac{N}{\sqrt{T_2}} \tag{A16}$$

From which the general relation is

$$\frac{\Delta w_f/\delta\sqrt{\theta}}{N/\sqrt{\theta}} = \frac{K_e C_p P_{STD}}{H} \cdot \frac{\Delta T_4}{T_2} \tag{A17}$$

APPENDIX B

AN ERROR ANALYSIS OF THE BASIC HYDROMECHANICAL METERING CIRCUIT

The volumetric output of the speed sensing pump can be expressed

$$Q = DN \pm \frac{\Delta P_R}{R_L} \tag{B1}$$

For ΔP_R positive, the flow error is

$$e = 100\left[\frac{Q - DN}{DN}\right] \tag{B2}$$

Substituting Eq. (B1)

$$e = \frac{100\,\Delta P_R}{R_L DN} \tag{B3}$$

The denominator of Eq. (B3) is the shut-off or dead-head pressure of the pump. The flow error is therefore proportional to the regulation error divided by the dead-head pressure. Because the forces acting on the pump gears are very small, the pump shafts can be cantilevered. This configuration makes very close gear to housing fits practical. The close fit provides the pump with a high theoretical value of dead head pressure. For this reason, errors of less than one percent are readily achievable.

The flow through the bypass can be written

$$Q_B = K A_B \sqrt{P_a - P_b} \tag{B4}$$

From Eq. (B4)

$$\frac{\partial Q_B}{\partial P_a} = \frac{K A_B}{2\sqrt{P_a - P_b}} \tag{B5}$$

The error in P_a is ΔP_R and for ΔP_R positive

$$\Delta Q_B = \frac{K A_B}{2\sqrt{P_a - P_2}} \Delta P_R$$

and

$$\frac{\Delta Q_B}{Q_B} = \frac{\Delta P_R}{2(P_a - P_b)} \tag{B6}$$

In the fuel control model currently in use on the Low-Cost Ordnance Technology engine, the maximum regulator error detected is 2 psi which occurs at maximum engine speed, where $(P_a - P_b)$ is 50 psi. From Eq. (B6) the error in bypass flow is two percent.

REFERENCES

1 Seldner, K., and Gold, H.: Computer and Engine Performance Study of a Generalized Parameter Fuel Control for Jet Engines. NASA TN D-5871, June 1970.

2. Batterton, P. G. and Gold, H.: Experimental Test Results of a Generalized-Parameter Fuel Control. NASA TN D-7198, March 1973.

3. Seldner, K.; Geyser, L. C.; Gold, H.; Walker, D.; and Burgner, G.: Performance and Control Study of a Low-Pressure-Ratio Turbojet Engine for a Drone Aircraft. NASA TM X-2537, April 1972.

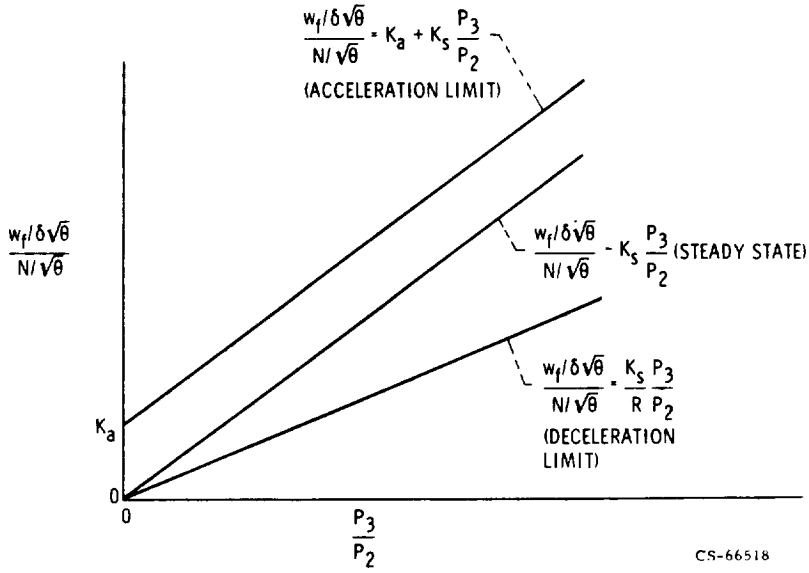

Figure 1. - Generalized acceleration and deceleration limit parameters.

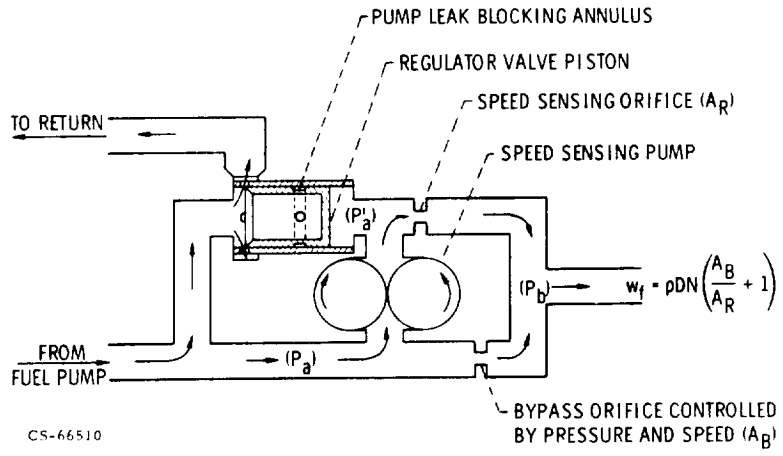

Figure 2. - Hydromechanical speed sensing and multiplying circuit.

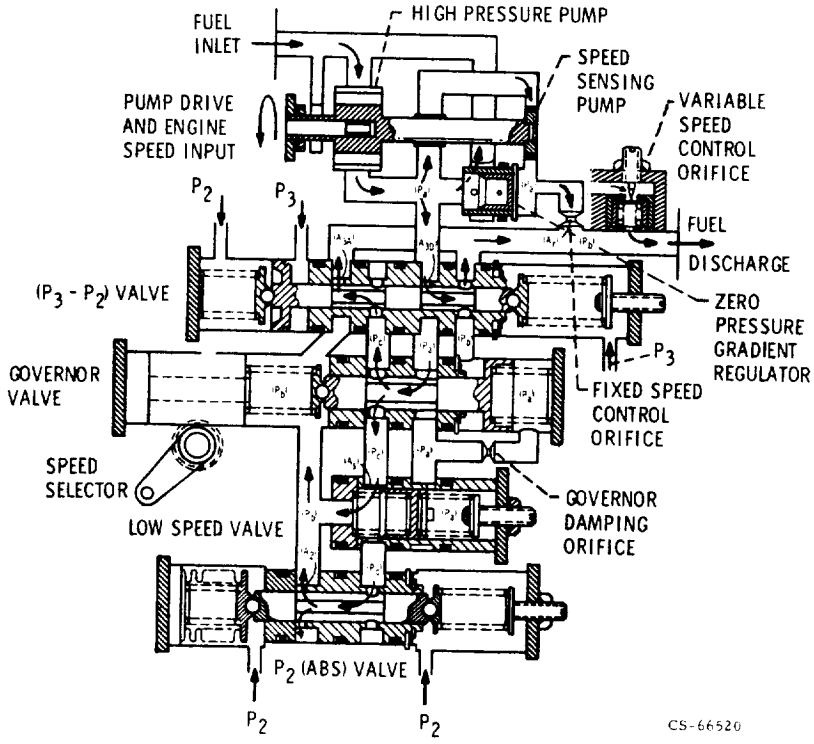

Figure 3. - Fuel control schematic diagram

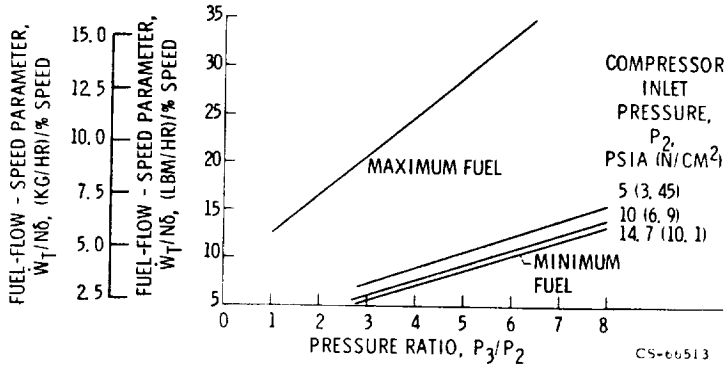

Figure 4. - Altitude effect on deceleration limit, simulated control for J85 engine.

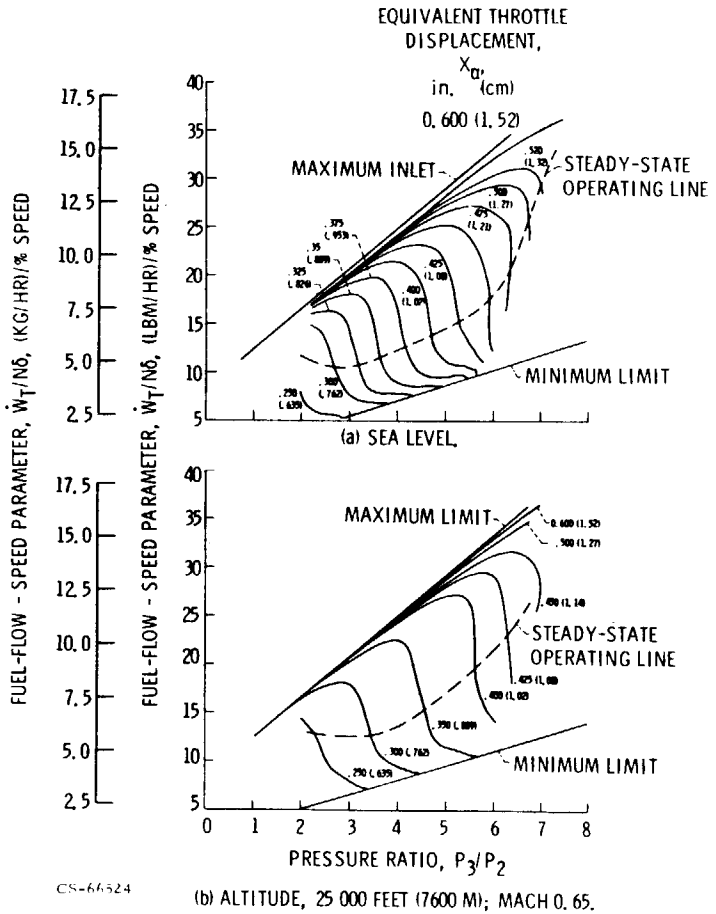

(b) ALTITUDE, 25 000 FEET (7600 M); MACH 0.65.

Figure 5. - Simulated J85 engine and fuel control characteristics in corrected parameter plane.

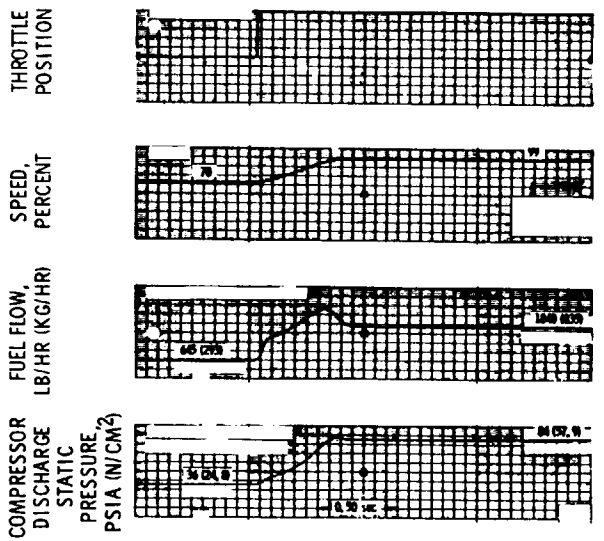

Figure 6. - Acceleration of the J85 engine at sea level with a simulated control.

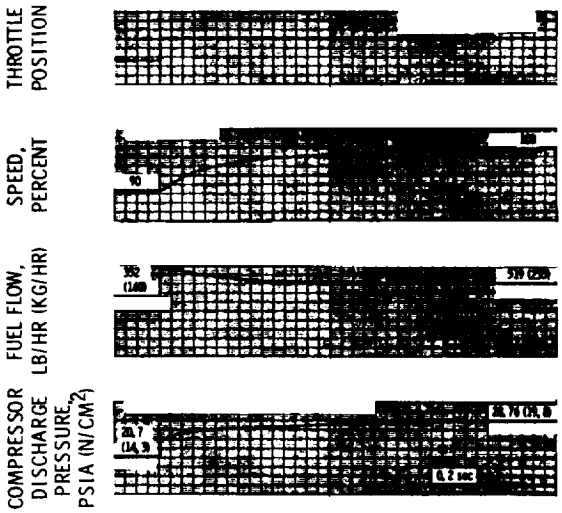

CS-66517

Figure 7. - Acceleration of simulated J85 engine at 40 000 feet, Mach 0.91, with a simulated fuel control.

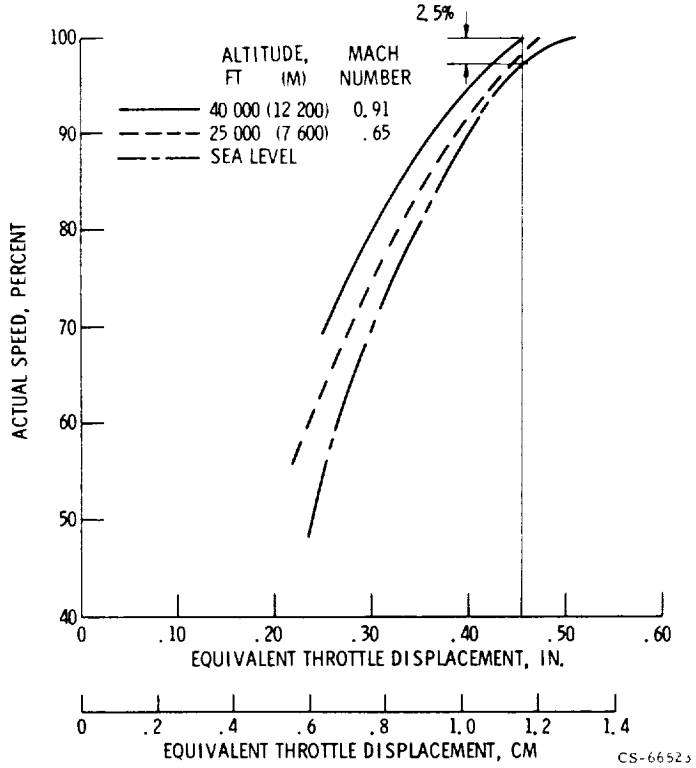

CS-66523

Figure 8. - Effect of altitude on governed speed, simulated J85 engine with simulated engine with simulated fuel control.

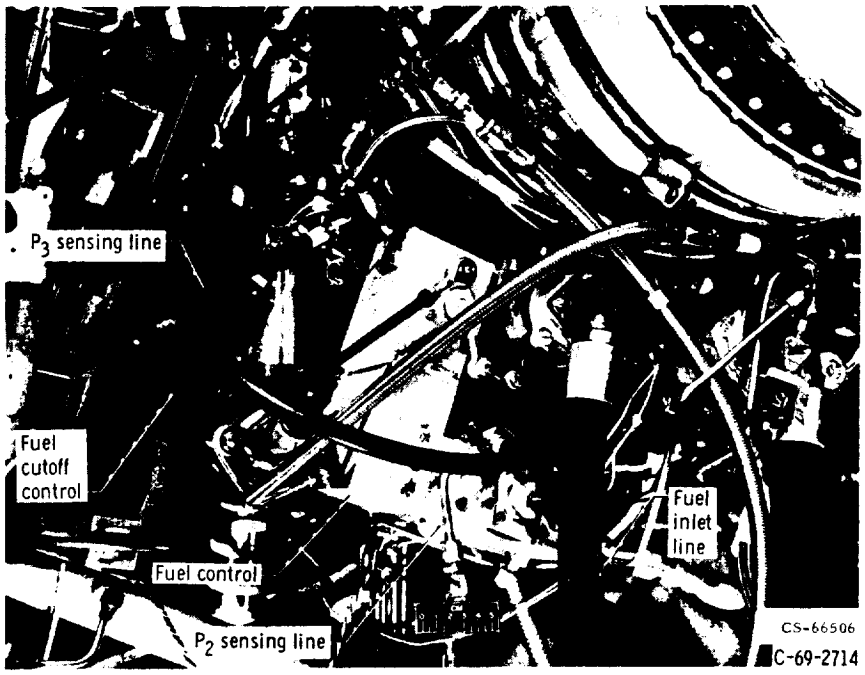

Figure 9. - Physical model of fuel control installed on J-85 engine.

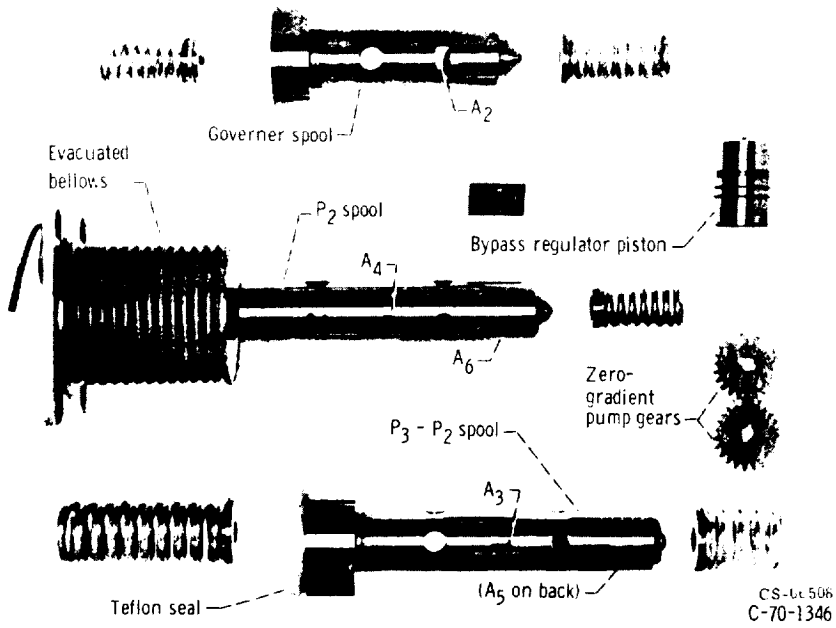

Figure 10. - Compenents of the physical model of the fuel control tested on the J-85 engine.

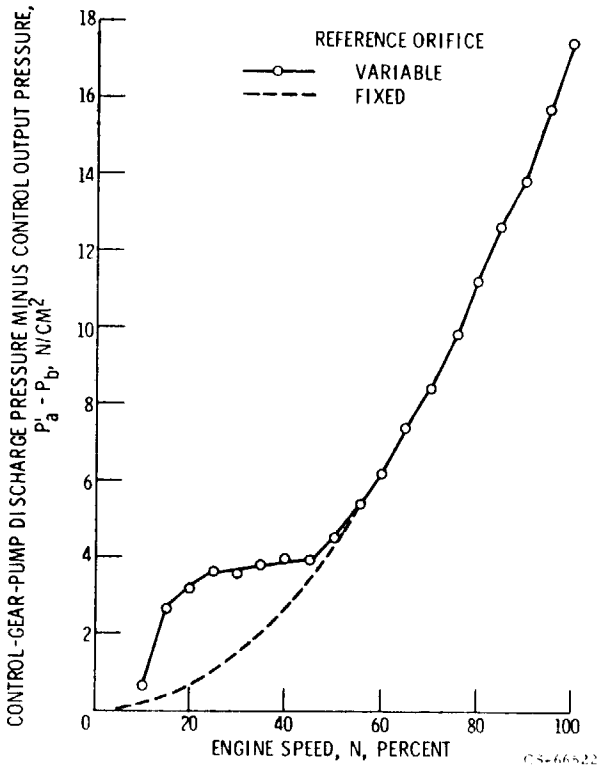

Figure 11. - Effect of variable speed sensing orifice on speed signal.

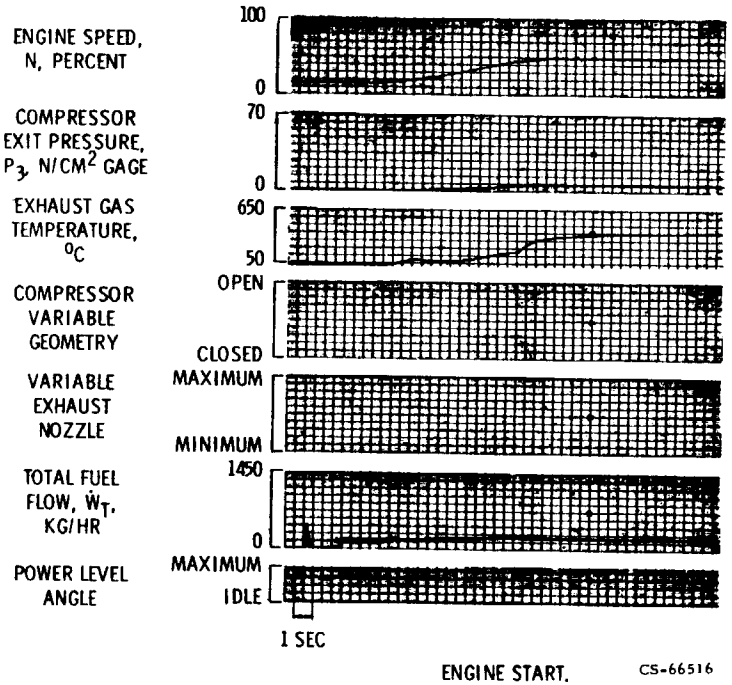

Figure 12. - Start of J85 engine with physical model of fuel control.

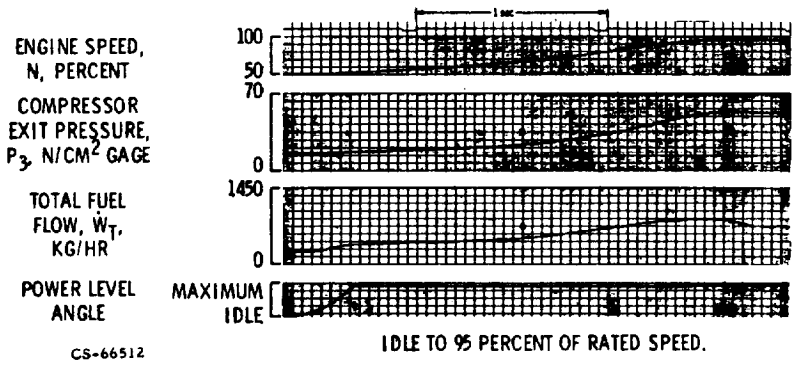

Figure 13. - Acceleration of the J85 engine at sea level with physical model of fuel control.

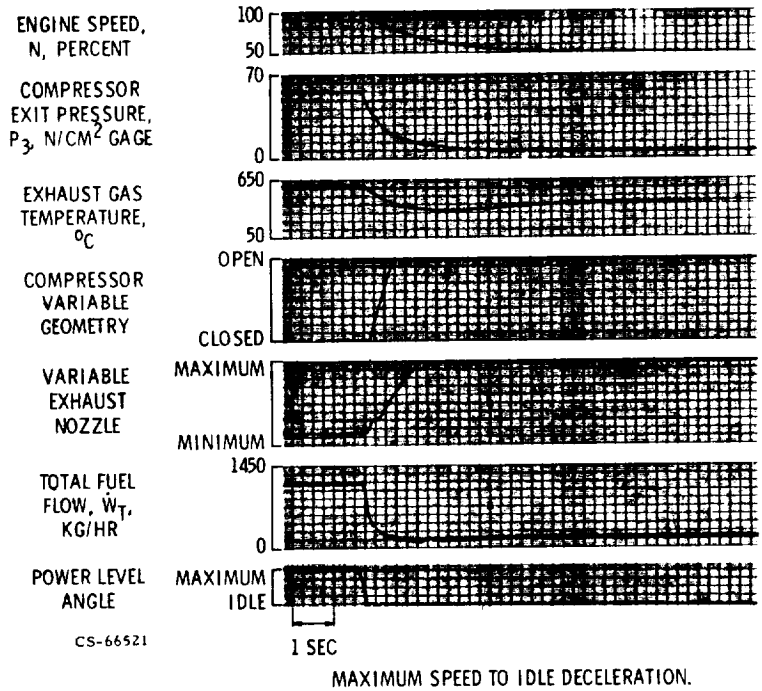

Figure 14. - Deceleration of the J85 engine at sea level with physical model of fuel control.

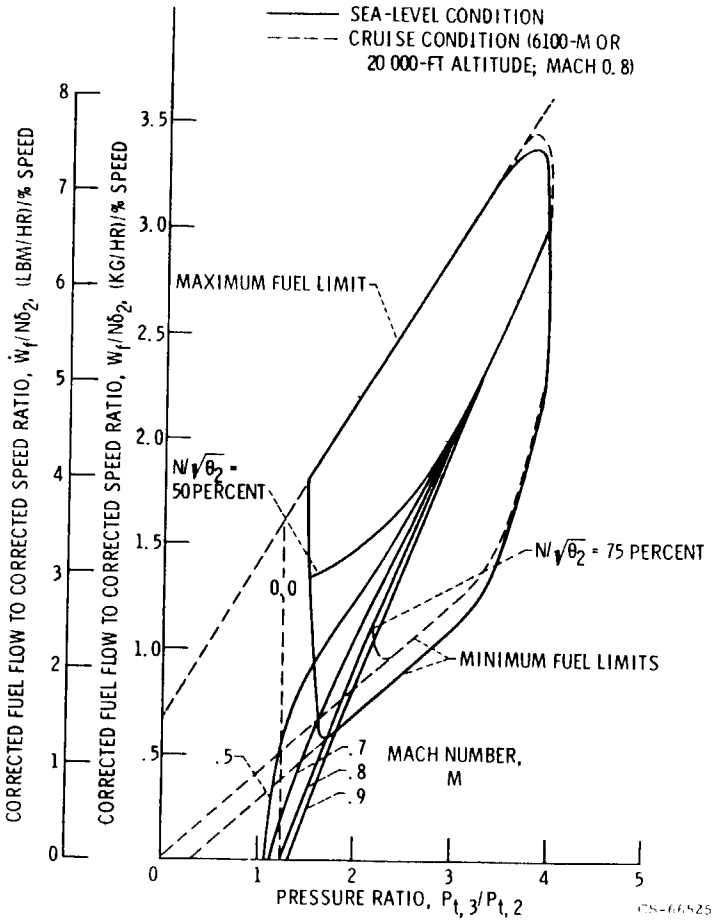

Figure 15. - Simulated low cost technology engine and fuel control characteristics in the corrected parameter plane.

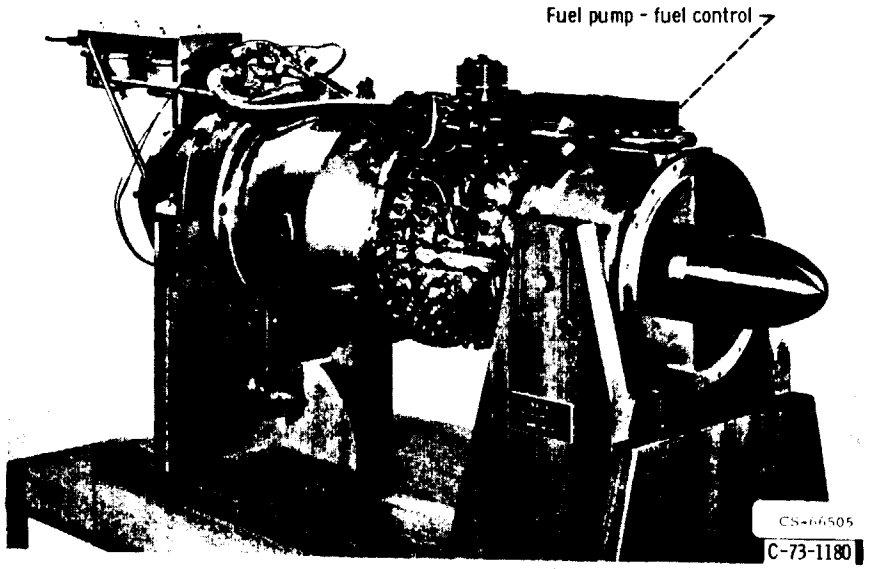

Figure 16. - Fuel control installed on Lewis low cost ordnance technology engine.

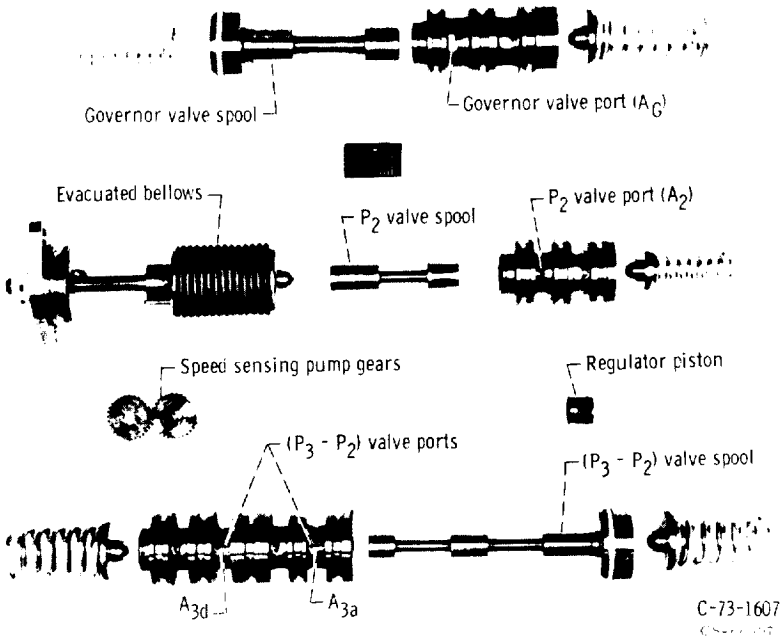

Figure 17. - Components of fuel control for low-cost ordnance technology engine.

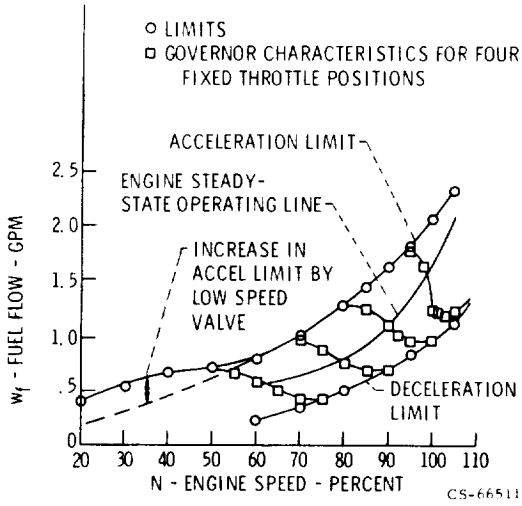

Figure 18. - Bench calibration low cost ordnance technology engine fuel control P_2 - 14.4 psia, T_2 - 520° R.

START OF LOW COST ORDNANCE TECHNOLOGY ENGINE WITH FUEL CONTROL

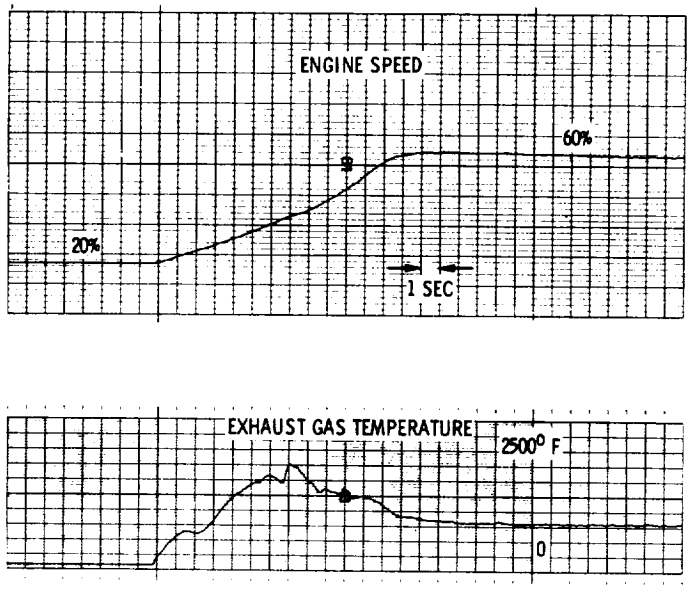

Figure 19. - Start of low cost ordnance technology engine with fuel control.

CS-66515

ACCELERATION OF LOW COST ORDNANCE TECHNOLOGY ENGINE
AT SEA LEVEL WITH FUEL CONTROL

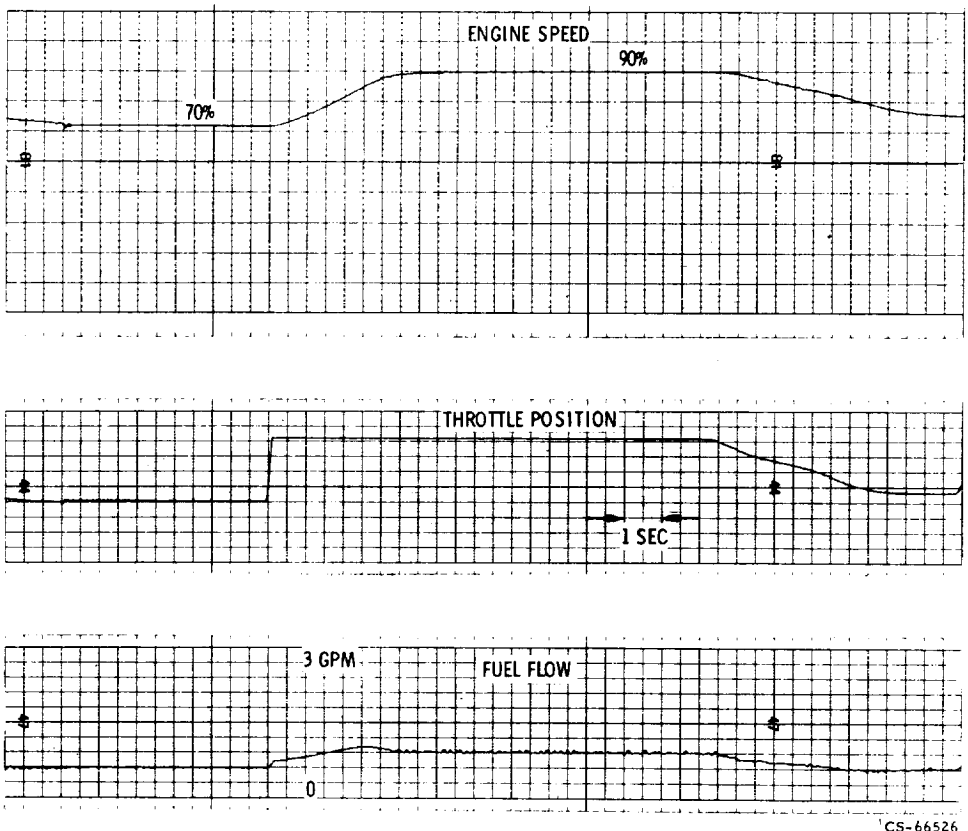

CS-66526

Figure 20. - Acceleration of low cost ordnance technology engine at sea level with fuel control.